energies

Article

Permanent Magnet Selections for AFPM Disc Generators

Natalia Radwan-Pragłowska * **and Tomasz Węgiel**

Faculty of Electrical and Computer Engineering, Cracow University of Technology, Warszawska 24 St., 31-155 Cracow, Poland
* Correspondence: natalia.radwan-praglowska@pk.edu.pl

Abstract: In this article, the field (FEM) and analytical analyses were used for the optimal selection of magnets material for the Axial Flux Permanent Magnet Generator (AFPMG), without building the prototype before. The tested generator is an axial flux machine which consists of a single stator and two rotor discs with Permanent Magnets (PM). Three-dimensional (3D) ANSYS Maxwell package was used for magnetostatic and transient field (FEM) simulations. Two types of PM were selected for the analysis: Ceramic (also known as "Ferrite") magnets made from Strontium Ferrite powder and Neodymium Iron Boron magnets (NdFeB). The authors compared obtained electromotive forces (EMF) and generator powers for selected magnets materials, performed FFT analyses of voltages and currents and indicated the optimal solutions. In addition to the operational properties of the AFPMG, the magnet and manufacturing costs were compared.

Keywords: permanent magnets; PM machines; axial flux PM generator; disk generator

check for updates

Citation: Radwan-Pragłowska, N.; Węgiel, T. Permanent Magnet Selections for AFPM Disc Generators. *Energies* **2022**, *15*, 7601. https://doi.org/10.3390/en15207601

Academic Editor: Marcin Wardach

Received: 26 August 2022
Accepted: 11 October 2022
Published: 14 October 2022

1. Introduction

The Permanent Magnet (PM) machines during the last years have become more popular, mainly because of the rapid development of the renewable energy industry and automotive applications. The usage of Permanent Magnets in the excitation circuit of synchronous machines allows us to increase their efficiency due to the lack of losses in excitation circuits compared to synchronous machines with classic electromagnetic excitation. This is a very important feature of this type of machine.

The Axial Flux Permanent Generators (AFPMG) have started to be commonly used in private, domestic wind turbines [1–4] but also in traction and low-speed drives [5,6], which is presented in other publications [7,8]. The operation of AFPMG depends on many aspects. Besides the generator's construction, one of the most significant factors is the magnet selection: volume, shape and the magnet type [9–21]. For this purpose, analytical models as well as field models (FEM) are used. Analytical models are very useful and are often used by engineers dealing with exploitation as well as by constructors in the initial stages of works [9–14].

Rare earth magnets of the NdFeB or SmCo type are usually used in the excitation circuits of electric machines. SmCo magnets are used less frequently and are dedicated to work in higher temperatures and corrosive aggressive environments, but their prices are extremely high. Recently, due to resource constraints and rising prices, trends in popularity of electrical machines without magnets but also in the elimination of rare earth Permanent Magnets have been noted. Considerations aimed at replacing rare earth magnets with other type of magnets, especially ceramic (Ferrite) magnets, were carried out in several works [22–38]. The biggest advantage of ceramic magnets is their low price, but at the same time, their significant drawback is the low level of magnetic properties (remanence, coercivity and maximum magnetic energy). Magnets with better magnetic properties compared to the ceramic magnets are rare earth magnets. NdFeB magnets have an optimal ratio of accumulated energy to mass and are resistant to demagnetization, but their weaknesses are their thermal properties (working temperature up to 200 °C) and poor corrosion tolerance [22,24,27–29,31,35,38]. Each magnet type has advantages and disadvantages. The PM proper selection depends on many aspects, such as funds, machine working conditions, desired magnet shapes and electrical parameters.

Analyses of replacing rare earth magnets (especially NdFeB) with ceramic magnets have been the subject of many studies [23,25,30,32–34,36,37], although most of the cases concerned machines with radial magnetic flux. These activities prompted the authors to carry out analyses related to the replacement of expensive NdFeB magnets by cheap ceramic (Ferrite) magnets for AFPMG design. As an example, the well-known AFPMG construction was selected, for which the authors performed the analyses and laboratory tests described in their previous works [39–41].

This work focuses on the AFPMG model construction with two rotor discs with Permanent Magnets (Figures 1 and 2) and one stator; however, these analyses can be also useful for other similar solutions. The basic assumption is that analysed generator belongs to the group of symmetrical three-phase disk generators excited by Permanent Magnets with a symmetrical structure. The main features of the AFPMG are: phase coils number p_s, total stator coils $3p_s$, one rotor side magnets number $4p_s = 2p$ (where p—pole pairs number, $p/p_s = 2$).

The main task of this article assumed by the authors is to check the possibility of replacing NdFeB magnets with another type of magnets for AFPMG, to analyse the costs and to show the suitability of the analytical model for using it in these types of considerations.

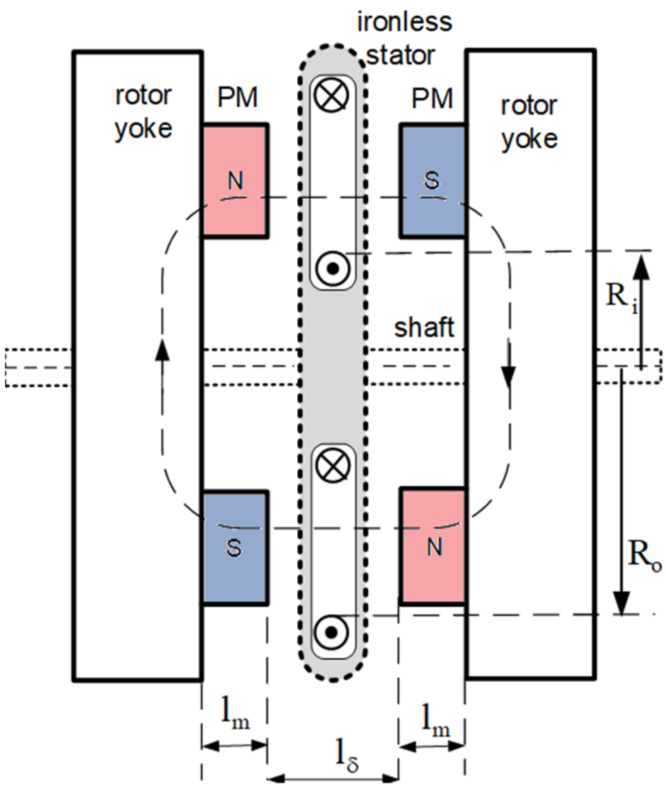

Figure 1. Double rotor AFPM generator construction.

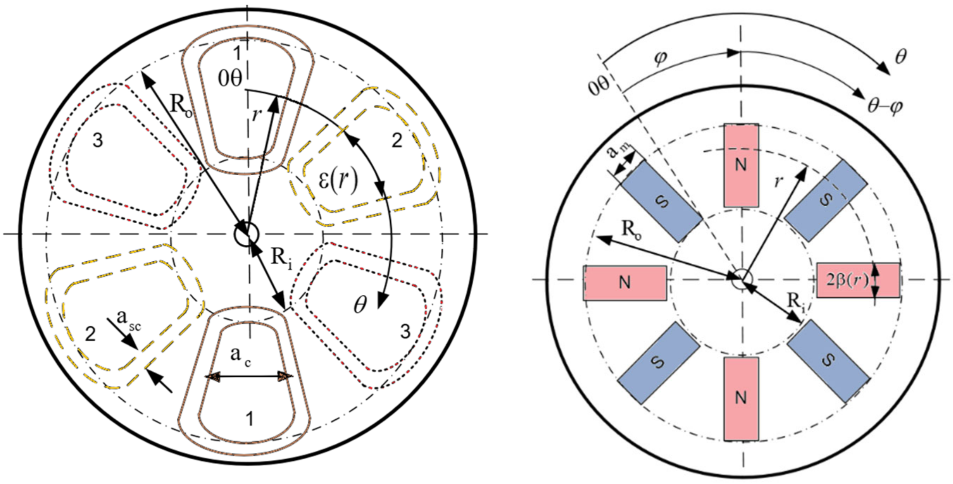

(**a**) (**b**)

Figure 2. (**a**,**b**) Exemplary Axial Flux Permanent Magnet Generator cross-section: (**a**) three-phase stator with non-overlapping winding (p_s = 2); (**b**) rotor disc (p = 4). Adapted from Ref. [39].

2. Mathematical Model

In this paper, a linear approximation of the Permanent Magnet demagnetization characteristics was assumed (according to Figure 3 where $B_m = B_r + \mu_0\mu_{rm}H_m$ and $\mu_{rm} = \frac{B_r}{\mu_0 H_0}$). To simplify considerations, the authors have also neglected the iron magnetic voltage drops. This dependence, according to occurring quantities, differ for selected magnet types, changing the magnetization curve influencing on the generator work.

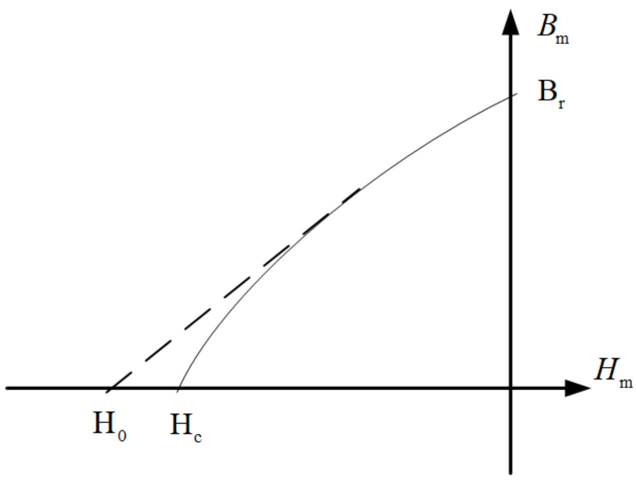

Figure 3. Demagnetization characteristics of Permanent Magnets.

For machines with a coreless disc structure and the rectangular magnets shape, basing on the exemplary literature [7,9–11,13,14,16,17,19,39,40], analytical formulas presenting the distribution of flux density in the air gap have been applied. The cross-section of AFPMG is presented in Figures 1 and 2, and Figure 4 presents a basic model defining symbols used to determine the magnetic field distribution.

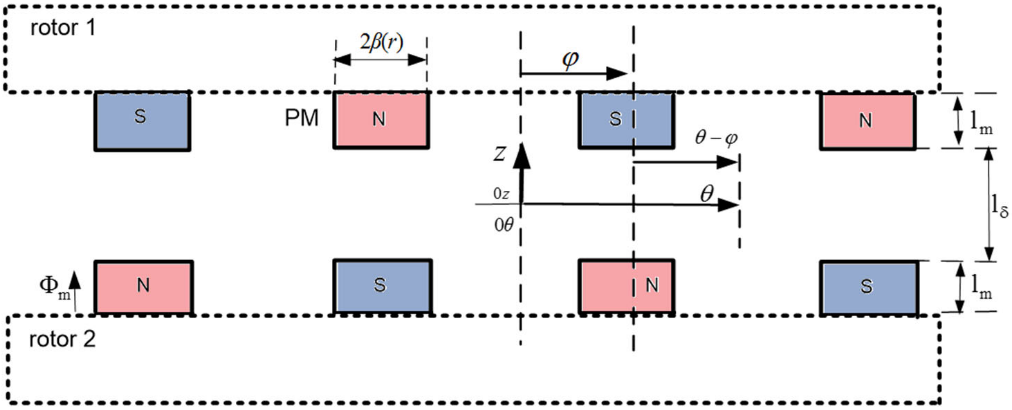

Figure 4. Schematic draw to define the distribution of magnetic field induced by PM.

In Figure 5 [39,40], the authors present the axial component approximation of magnetic flux-density distribution (for the middle of the air gap, which means that $z = 0$), which refers to the coreless AFPM generator induced by the Permanent Magnets.

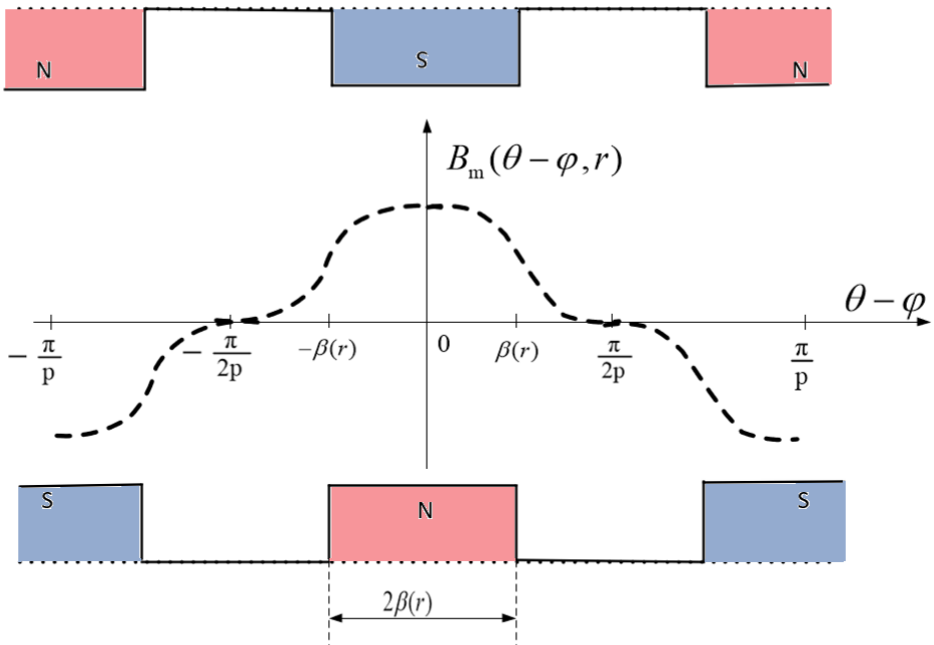

Figure 5. Approximated distribution function of magnetic flux-density from PM in the air gap according to $\theta - \varphi$; Model 2D—dashed curve. Adapted from Ref. [39].

Using the Fourier series, the magnetic flux-density distribution in the gap induced by Permanent Magnets can be approximated by [9,11,39,40]:

$$B_{\mathrm{m}}(\theta - \varphi, r) = \sum_{\varsigma \in \{\ldots -5\mathrm{p}, -3\mathrm{p}, -\mathrm{p}, \mathrm{p}, 3\mathrm{p}, 5\mathrm{p}, \ldots\}} B_{\varsigma}^{\mathrm{PM}}(r) \cdot \mathrm{e}^{\mathrm{j}\varsigma(\theta - \varphi)} \quad (1)$$

Fourier coefficients $B_{\varsigma}^{\mathrm{PM}}(r)$ can be presented using a two-dimensional (2D) model of the magnetic field distribution [9,11,39,40]:

$$B_{\varsigma}^{\mathrm{PM}}(r) = \frac{2\,\mathrm{B_r}}{\pi}\frac{\mathrm{p}}{\varsigma} \cdot \sin(\varsigma \cdot \beta(r)) \frac{2\sinh(\varsigma \frac{\mathrm{l_m}}{r}) \cdot \cosh(\varsigma \frac{2\,\mathrm{l_m} + \mathrm{l_\delta}}{2r})}{\mu_{\mathrm{rm}} \cdot \sinh(\varsigma \frac{\mathrm{l_\delta} + 2\,\mathrm{l_m}}{r})} \quad (2)$$

Basing on [39,40], the three-phase AFPMG mathematical model can be presented in a standard matrix form, according to Lagrange formalism:

$$\begin{bmatrix} L_{\sigma s}+L_{ss} & & \\ & L_{\sigma s}+L_{ss} & \\ & & L_{\sigma s}+L_{ss} \end{bmatrix} \cdot \frac{\mathrm{d}}{\mathrm{d}t} \begin{bmatrix} i_1 \\ i_2 \\ i_3 \end{bmatrix} + R_s \cdot \begin{bmatrix} i_1 \\ i_2 \\ i_3 \end{bmatrix} + \frac{\mathrm{d}\varphi}{\mathrm{d}t} \cdot \frac{\partial}{\partial\varphi} \begin{bmatrix} \psi_{\mathrm{PM}\,1}(\varphi) \\ \psi_{\mathrm{PM}\,2}(\varphi) \\ \psi_{\mathrm{PM}\,3}(\varphi) \end{bmatrix} = \begin{bmatrix} u_1 \\ u_2 \\ u_3 \end{bmatrix} \quad (3)$$

$$J\frac{\mathrm{d}^2\varphi}{\mathrm{d}t^2} = T_{\mathrm{L}} + T_{\mathrm{em}}(i_1, i_2, i_3, \varphi) - D\frac{\mathrm{d}\varphi}{\mathrm{d}t} \quad (4)$$

where the electromagnetic torque T_{em}:

$$T_{\mathrm{em}}(i_1, i_2, i_3, \varphi) = \begin{bmatrix} i_1 & i_2 & i_3 \end{bmatrix} \cdot \frac{\partial}{\partial\varphi} \begin{bmatrix} \psi_{\mathrm{PM}\,1}(\varphi) \\ \psi_{\mathrm{PM}\,2}(\varphi) \\ \psi_{\mathrm{PM}\,3}(\varphi) \end{bmatrix} \quad (5)$$

The above equations are obvious but considering the presence of Permanent Magnets in the generator magnetic circuit, some changes should be introduced to the basic parameters compared to classic models.

Considering $r \approx \mathrm{r_s} = \frac{\mathrm{R_o}+\mathrm{R_i}}{2}$ allowed the authors to simplify the analysis. The flux $\psi_{\mathrm{PM}\,a}$ linked with winding 'a', generated by PM in zero current state, can be defined using the standard formula:

$$\psi_{\mathrm{PM}\,a}(\varphi) = \sum_{\varsigma \in \{\ldots -5\mathrm{p}, -3\mathrm{p}, -\mathrm{p}, \mathrm{p}, 3\mathrm{p}, 5\mathrm{p}, \ldots\}} \psi_{\varsigma}^{\mathrm{PMs}} \cdot \mathrm{e}^{\mathrm{j}\varsigma\{(a-1)\frac{4\pi}{3\mathrm{p}} - \varphi\}} \quad \text{for } a = 1,2,3 \quad (6)$$

and the winding 'a' electromotive force (EMF) at constant speed and zero current state, can be described by the following equation:

$$e_{\mathrm{PM}a} = \sum_{\varsigma = \mathrm{p}, 3\mathrm{p}, 5\mathrm{p}\ldots} E_{\varsigma} \cdot \cos\varsigma\{\Omega t - (a-1)\frac{4\pi}{3\mathrm{p}}\} \text{ for } a = 1,2,3 \quad (7)$$

where: $E_{\varsigma} = 2\varsigma\ \Omega\ \psi_{\varsigma}^{\mathrm{PMs}}$ and Ω is the angular speed (rad/s).

The coefficients distribution function of the flux produced by Permanent Magnets linked with the stator winding and Equation (6) must be modified considering the weakening of the flux at the magnets' edges. For the disc generator with the coreless stator and a relatively large air gap, this fact is important in the quantitative analysis. Based on considerations contained in [40], the authors proposed a correction factor k_{e}:

For the cases where:

$$\mathrm{l_c} > (\mathrm{l_m} + \mathrm{l_\delta}):\ k_{\mathrm{e}} = \frac{\sum_{\varsigma \in \{\ldots -5\mathrm{p}, -3\mathrm{p}, -\mathrm{p}, \mathrm{p}, 3\mathrm{p}, 5\mathrm{p}, \ldots\}} B_{\varsigma}^{\mathrm{PM}}(\mathrm{r_s}) \cdot [1 - (1 - \frac{2}{\pi})\frac{\mathrm{l_m}+\mathrm{l_\delta}}{2\mathrm{l_c}}]}{\sum_{\varsigma \in \{\ldots -5\mathrm{p}, -3\mathrm{p}, -\mathrm{p}, \mathrm{p}, 3\mathrm{p}, 5\mathrm{p}, \ldots\}} B_{\varsigma}^{\mathrm{PM}}(\mathrm{r_s}) \cdot \frac{\sin\varsigma\beta(\mathrm{r_s})}{\varsigma\beta(\mathrm{r_s})}} \quad (8)$$

and for the cases where:

$$\mathrm{l_c} < (\mathrm{l_m} + \mathrm{l_\delta}):\ k_{\mathrm{e}} = \frac{\sum_{\varsigma \in \{\ldots -5\mathrm{p}, -3\mathrm{p}, -\mathrm{p}, \mathrm{p}, 3\mathrm{p}, 5\mathrm{p}, \ldots\}} B_{\varsigma}^{\mathrm{PM}}(\mathrm{r_s}) \cdot (\frac{1}{2} + \frac{1}{\pi})}{\sum_{\varsigma \in \{\ldots -5\mathrm{p}, -3\mathrm{p}, -\mathrm{p}, \mathrm{p}, 3\mathrm{p}, 5\mathrm{p}, \ldots\}} B_{\varsigma}^{\mathrm{PM}}(\mathrm{r_s}) \cdot \frac{\sin\varsigma\beta(\mathrm{r_s})}{\varsigma\beta(\mathrm{r_s})}} \quad (9)$$

where: $\mathrm{l_c} = \mathrm{R_o} - \mathrm{R_i}$—the magnet length.

For the coreless generator, assuming that the relative magnetic permeability of PM is close to the magnetic permeability of air ($\mu_{rm} \cong 1.01 \ldots 1.1$), the function distribution of unit permeability can be approximated just by the constant component:

$$\lambda_0 = \lambda_{min} + \frac{2p\beta(r_s)}{\pi}(\lambda_{max} - \lambda_{min}) \tag{10}$$

where:

$$\lambda_{min} = \frac{\mu_0}{l_\delta + 2l_m};\ \lambda_{max} = \frac{\mu_0}{l_\delta + 2l'_m};\ l'_m = \frac{l_m}{\mu_{rm}}$$

The improved flux linkages coefficients induced by PM (6) can be described as:

$$\psi_\varsigma^{PMs} = 2\ k_e \cdot B_\varsigma^{PM}(r_s)\ \cdot W_\varsigma^s(r_s)\ \cdot r_s \cdot l'_c \frac{\lambda_{max}}{\lambda_0} \tag{11}$$

where:

$$W_\varsigma^s(r_s) = \frac{w_s \cdot k_s^{|\varsigma|}(r_s)}{|\varsigma|} \tag{12}$$

w_s—the whole turns number of the stator phase winding,
$k_s^{|\varsigma|}$—the winding factor for ς^{th} harmonic [7,39,40]:

$$k_s^{|\varsigma|}(r_s) = \sin(|\varsigma|\frac{\varepsilon(r_s)}{2}) \cdot \frac{\sin(|\varsigma|\frac{\alpha_{sc}(r_s)}{2})}{|\varsigma|\frac{\alpha_{sc}(r_s)}{2}} \tag{13}$$

$\varepsilon(r_s) = \frac{a_c}{r_s}$—coil pitch angle or coil span at coordinate $r = r_s$,
$\alpha_{sc}(r_s) = \frac{a_{sc}}{r_s}$—an angle of the coil side width at coordinate $r = r_s$,
l'_c—length of the active side of the coil and in most cases $l'_c \approx R_o - R_i$.
To define the windings inductances, the authors used standard relationships [7,8,39,40]:

$$L_{ss} = \sum_{\nu \in \{\ldots -3p_s, -2p_s, -p_s, p_s, 2p_s, 3p_s, \ldots\}} \frac{2}{\pi} \cdot [W_\nu^s(r_s)]^2 \cdot r_s \cdot l'_c \cdot \lambda_0 \tag{14}$$

The analytical description of leakage inductances can be defined as the sum of two components [25]. The first one refers to the leakage flux around the active conductors' radial part (coil sides) and the second one is related to the leakage flux around the end windings. The leakage inductance coefficient can be expressed by the following equation:

$$L_{\sigma s} \approx 2\mu_0 \cdot (w_s)^2\ [l'_c + (a_c - a_{sc})]\ \cdot 0.3/p_s \tag{15}$$

The presented mathematical model can be used to show the influence of the selected magnet type on the magnetic flux density and EMF, which will be discussed in this article in accordance with the field analysis (FEM).

3. Case Study of Replacing NdFeB Magnets by Ceramic Magnets

3.1. FEM Model Description

The analysed generator consists of a single, coreless stator with 21 coils and two rotor discs. Each rotor disc has 28 (surface mounted) Permanent Magnets.

The structure of the tested generator, modelled in ANSYS Maxwell software, is presented in Figure 6 and in Table 1. The FEM analysis was performed using the ANSYS Maxwell software. The transient and magnetostatic analysis methods were used. The work temperature was set to 22 °C. The total number of mesh elements was 857,643 (compaction depends on the element). The assumed rotational speed was 206 rpm (48 Hz). The authors also had at their disposal the previously discussed [39–41] laboratory model of the generator, with NdFeB magnets (Figure 7), which served as a reference point in the presented analyses.

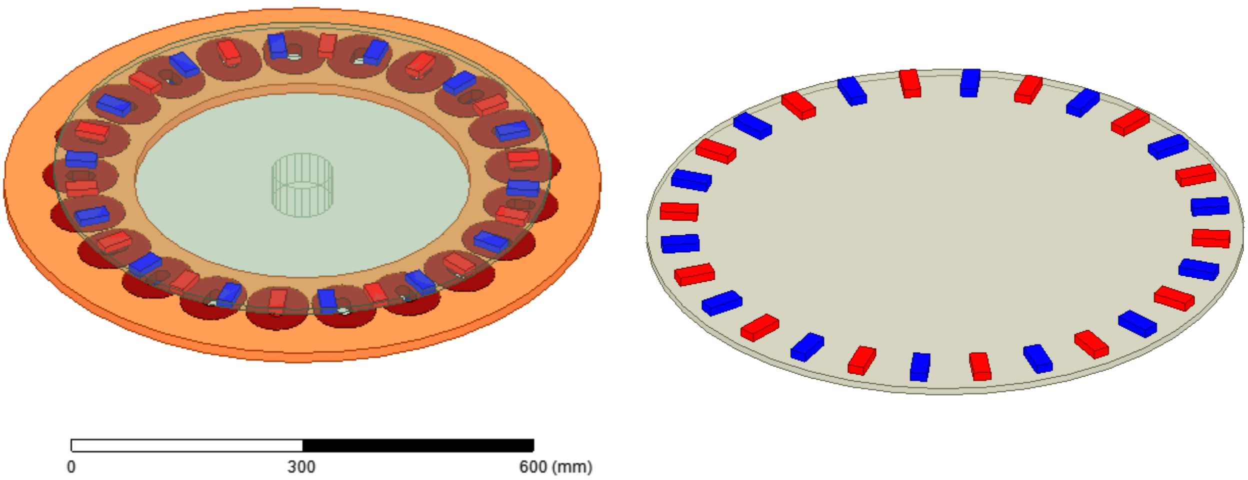

(**a**) (**b**)

Figure 6. AFPMG with non-overlapping windings in ANSYS Maxwell software: (**a**) Generator model; (**b**) Rotor disc with PM arrangement.

(**a**) (**b**)

Figure 7. Laboratory model of AFPMG with NdFeB magnets: (**a**) Stator disk; (**b**) Rotor disk.

Table 1. Construction data.

AFPMG Design Parameters and Dimensions	
Main dimensions:	R_i = 270 mm; R_o = 310 mm; r_s = 290 mm
Stator and rotor outer diameter:	780 mm/650 mm
Number of phase coils:	p_s = 7; Total number of stator coils: 21
Total number of phase winding turns:	w_s = 980
Stator winding coil dimensions:	l'_c = 42 mm; a_c = 50 mm; a_{sc} = 30 mm; $\alpha_{sc}(r_s)$ = 0.1034 rad; $\varepsilon(r_s)$ = 0.1517 rad
Length of equivalent air gap:	l_δ = 26 mm
Stator winding resistance:	R_s = 2 Ω
Rotor magnets number (per rotor disc):	28; p = 14
Dimensions of a basic, single magnet:	l_m = 10 mm or 30 mm (for Ceramic enlarged); a_m = 18 mm; $\beta(r_s)$ = 0.0290 rad; l_c = 40 mm

This work focuses on two magnet types, such as: Ceramic magnets (Ferrite) made from Strontium Ferrite powder and Neodymium Iron Boron ones (NdFeB). The main parameters of selected Permanent Magnets such as coercive force, remanence, and relative permeability, used in ANSYS Maxwell simulations, are presented in Table 2.

Table 2. Magnets data used in ANSYS Maxwell.

PM	Coercive Force H_c ($H_0 \approx H_c$)	Residual Flux Density B_r	Relative Permability μ_{rm}
Ceramic 8	267 kA/m	0.4 T	1.19
NdFeB	899 kA/m	1.2 T	1.07

3.2. Analysis of Models with Identical and Different Magnets Size

The first analysis was obtained for block magnets with the same size (10 × 18 × 40 mm) for all magnet materials. The detailed mathematical description of the flux density distribution and determining the EMF for this model construction was fully described in [9,11,19,40] and briefly discussed in Formulas (1)–(12), pointing the influence of the magnets' parameters on output parameters. The flux density plots (for the whole generator and selected Permanent Magnets) obtained from 3D magnetic analysis for selected magnet types are shown in Figure 8a,b.

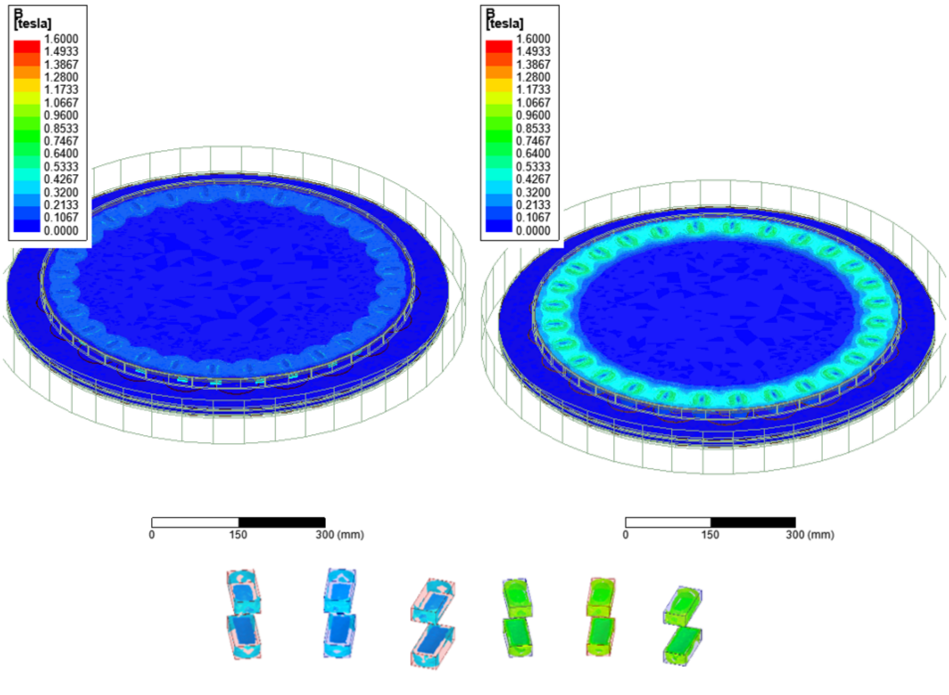

(**a**) (**b**)

Figure 8. Magnetic flux density for different magnet types: (**a**) Ceramic; (**b**) NdFeB.

To obtain a higher output voltage and compare the total magnets price for analysed construction, the authors performed further tests with different magnet volumes. The assumed ceramic magnets height was three time bigger then NdFeB magnets while the width and length were constant. The electromotive forces (EMF) and stator currents were obtained from FEM transient analysis for selected magnet types and sizes are shown in Figures 9 and 10. The presented spectra (in dB) are for the adopted reference levels: 1 mV for voltages; 0.1 mA for currents.

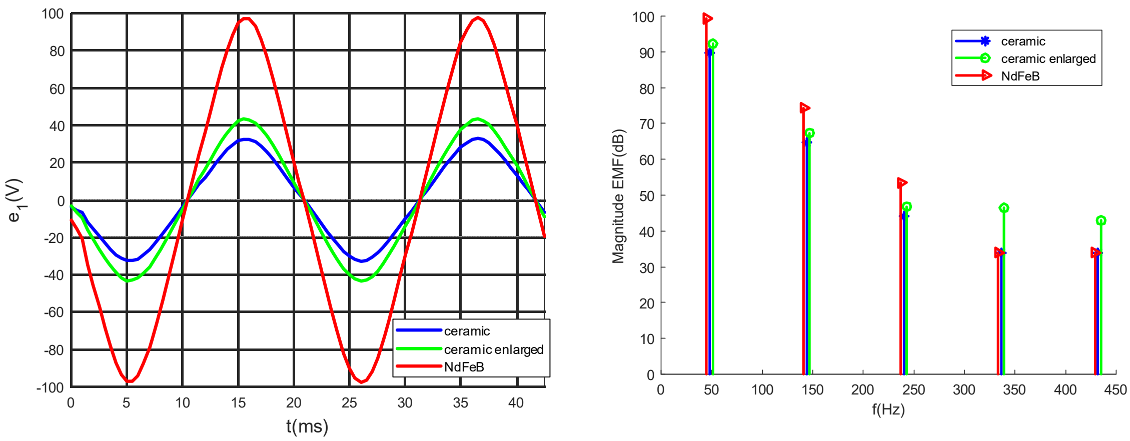

(**a**) (**b**)

Figure 9. Induced EMF (phase 1) for different magnet types: Ceramic; Ceramic enlarged and NdFeB (**a**) Waveform of EMF; (**b**) FFT spectrum of EMF.

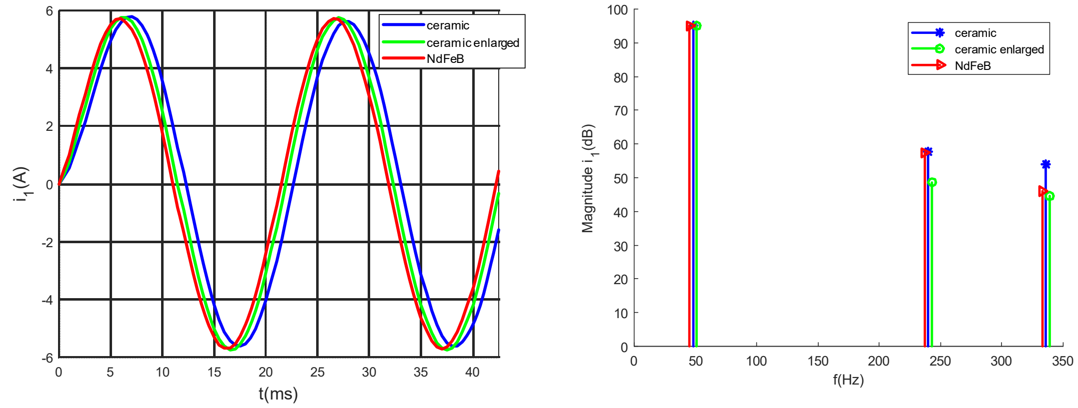

(**a**) (**b**)

Figure 10. Stator current (phase 1) for generator at nominal load for different magnet types: Ceramic; Ceramic enlarged and NdFeB (**a**) Waveform; (**b**) FFT spectrum.

The obtained electromotive force for AFMPG is visibly the highest with the usage of NdFeB magnets for rotor discs variant. Table 3 shows the voltage RMS value ($E_{\mathrm{G\ ph\ (RMS)}}$) obtained by FEM and analytical calculations and approximate price for one item of basic magnets size (block magnets) from above considerations.

Table 3. Analysis results and prices for 10 May 2022 [42,43].

AFPMG	Size	Volume	$E_{\mathrm{G\ ph\ (RMS)}}$ FEM	$E_{\mathrm{G\ ph\ (RMS)}}$ Analytical	Approx. Price for 1 Item	Approx. Total Price
Ceramic	10 × 18 × 40 mm	7.2 cm^3	21.9 V	20.4 V	0.5 $	28 $
Ceramic enlarged	30 × 18 × 40 mm	21.6 cm^3	29.6 V	28.1 V	1.5 $	84 $
NdFeB	10 × 18 × 40 mm	7.2 cm^3	65.4 V	63.9 V (62.6 V measured)	6 $	336 $

From analysing Table 3, one can see a big influence of magnet type on EMF ($E_{\mathrm{G\ ph\ (RMS)}}$). By changing the magnet type from ceramic to NdFeB, it is possible to increase the obtained EMF value by about three times. Comparing the prices, it is worth checking the magnet's size influence on the induced voltage and compare the total price per one item. Comparing the obtained RMS voltage value and the total price, the NdFeB magnets seem to be the optimal choice. In the case of ceramic magnets, further size increasing has not significantly increased the induced EMF.

Table 4 shows the comparison of obtained THD values of the generator electromotive force ($E_{\mathrm{G\ ph\ (RMS)}}$) and stator phase current ($I_{\mathrm{G\ ph\ (RMS)}} = I_{\mathrm{GN}}$), according to selected sizes and magnet materials.

Table 4. Comparison of the THD coefficient obtained from FEM model for EMF and current i_1.

AFPMG	$\mathrm{THD_{EMF}}$	$\mathrm{THD_I}$
Ceramic	5.6%	1.6%
Ceramic enlarged	5.8%	0.6%
NdFeB	5.7%	1.4%

Analysing the results from Table 4, it can be seen that changes in the size and type of magnets do not significantly affect the deformation and the appearance of higher harmonics of induced voltages (EMF) and phase currents.

3.3. Comparisons of AFPMG with Ceramic and NdFeB PM

In the next step, the generator models with ceramic magnets (for basic and enlarged size) and NdFeB (with the basic size) were analysed under resistive loads. The following Figures 11 and 12 present external characteristics of AFPMG with different magnet sizes and materials for the generator under a resistive load. Figure 11 shows generator voltage characteristics as a function of stator current U_G = f(I_G) and Figure 12 shows the dependence of generated power P_G = f(I_G) as a function of the current for selected magnet types.

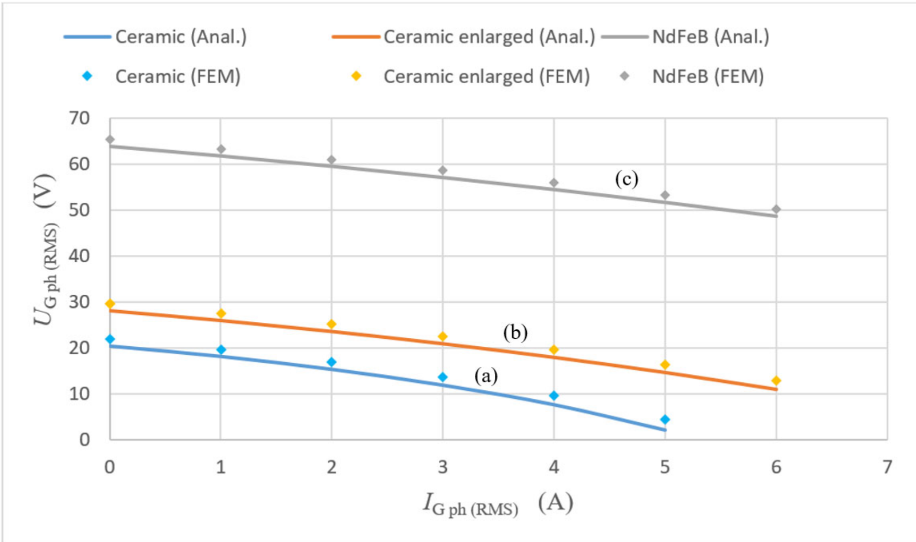

Figure 11. Generator voltage changes as a function of current: (**a**) Ceramic basic size; (**b**) Ceramic enlarged; (**c**) NdFeB basic size.

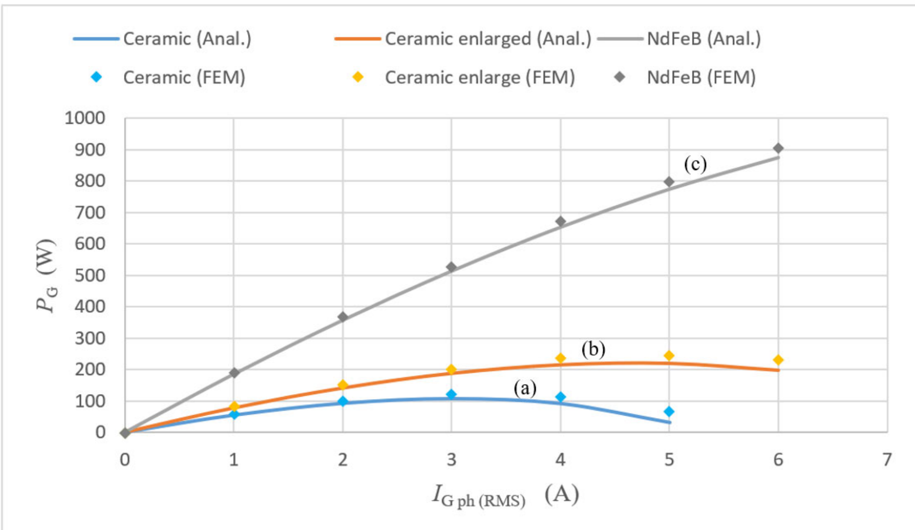

Figure 12. Generator power as a function of current: (**a**) Ceramic basic size; (**b**) Ceramic enlarged; (**c**) NdFeB basic size.

From analysing Figure 11, one can see that the generator voltage drop is smaller for the NdFeB (about 14%) and ceramic magnets with enlarged size (about 34%) than in the case of ceramic magnets with the basic size (about 56%) for current load $I_{\text{G ph (RMS)}} = 4$ A.

At Figure 12 it can be seen that enlarging the ceramic magnets height by three times gives almost 100% more power that in the case of basic size ceramic magnets, which means that one can finally achieve about 250 W.

Table 5 shows the comparison of obtained phase voltages $U_{\text{G ph (RMS)}}$ and generator power P_{G} for the same nominal value of stator current $I_{\text{G ph (RMS)}} = I_{\text{GN}}$, according to Figures 11 and 12. The fixed cost of manufacturing the machine was assumed at the level of 200 $ (rotor iron discs, stator and coils, bearings, shaft, housing) which, after adding the price of the magnets, gave the total cost of the generators.

Table 5. Comparison of $U_{\text{G ph (RMS)}}$ and P_{G} for same I_{GN} value and costs of generators.

AFPMG	I_{GN}	$U_{\text{G ph (RMS)}}$ FEM	$U_{\text{G ph (RMS)}}$ Analytical	P_{G} FEM	Generator Total Price	Price of Generator 1W Power
Ceramic	4.0 A	9.7 V	8.6 V	114 W	228 $	2 $
Ceramic enlarged	4.0 A	19.1 V	18.0 V	235 W	284 $	1.2 $
NdFeB	4.0 A	55.3 V	54.5 V	672 W	536 $	0.8 $

Based on the analysis of the data in Table 5, it can be concluded that increasing the size of the ceramic magnets leads to a 100% increase in the generator power with a slight increase in cost. The generator with enlarged ceramic magnets is almost two times cheaper than one with NdFeB magnets; however, the power obtained is three times lower. Furthermore, while converting the total costs of generator production into watts of received power in the case of generator design with NdFeB magnets, one can obtain an approximately 50% cheaper solution than in the case of ceramic enlarged magnets.

4. Conclusions

The Permanent Magnets are commonly used in machines designed in the recent years. The proper magnet selection has the significant influence on the work of Permanent Magnet Machines. However, one should remember about the economic aspect of constructed generators and the conditions in which Permanent Magnets can be installed. The main goal of the presented approach was to use an analytical model that allows for an effective analysis of electromagnetic phenomena while checking if it is possible to replace the rare earth magnets in AFPMG construction.

The authors have made the research on disk generators, based on the FEM and analytical models, using the ceramic magnets (Ferrite) made from Strontium Ferrite powder and Neodymium Iron Boron ones (NdFeB). The use of the following magnet types for analysis: Samarium Cobalt (SmCo) magnets, Aluminum, Nickel, and Cobalt (AlNiCo) magnets, were rejected due to their high prices. Considering the obtained results, one can see that by changing the magnet type it is possible to obtain several times higher power of the PM machines. However, it is also important to get the optimum output parameters while maintaining the right total price. SmCo magnets have similar features compared to NdFeB and can be successfully used in marine, aerospace, and industrial automation areas, because they do not need to be additionally protected against corrosion. They also allow us to obtain a rather good generator output power compared to the ceramic magnets. They have high corrosion resistance and high energy at the same time. Yet, a significant disadvantage is the fact that they are much more expensive than NdFeB magnets, which is why the authors did not take them into the consideration.

Considering the gained output voltage and magnet price, NdFeB magnets seem to be the best choice, especially while building small, domestic power plants. At the same time, when choosing Neodymium magnets for disc generators, it is necessary to avoid acidic, alkaline, and humid environment, according to their tendency to oxidize. The shape limit of NdFeB magnets can be expanded by connecting single magnets into some more arrangements. Because they are the strongest Permanent Magnets, NdFeB are appropriate for constructions which require limited generator dimensions with a high output power at the same time.

For economical, domestic constructions, when the high output power is not expected, one can use the ceramic magnets. They are limited to single shapes but are the cheapest ones. Enlarging the ceramic magnets' height enables us to obtain about 100% more power than in the case of the first analysed size. Unfortunately, comparing the total generator price, and converting the costs production into one watt, the difference is in favour of NdFeB.

In conclusion, it can be noted that for the analysed generator structure (AFPMG) with rare earth and ceramic magnets, the analytical model is also effective. The obtained discrepancies in the results obtained from the analytical models compared to the FEM analyses were within the range of 10%.

However, replacing NdFeB magnets with ceramic magnets is not the most optimal solution; yet, it may be acceptable in low-power structures such as home micro wind or hydroelectric power plants.

Author Contributions: Conceptualization, N.R.-P. and T.W.; methodology N.R.-P. and T.W.; validation, N.R.-P. and T.W.; investigation, N.R.-P. and T.W.; data curation, N.R.-P. and T.W.; writing—original draft preparation, N.R.-P. and T.W.; writing—review and editing, N.R.-P. and T.W.; supervision, N.R.-P. and T.W. All authors have read and agreed to the published version of the manuscript.

Funding: This work presented in this paper was funded by subsidies on science granted by Polish Ministry of Science and Higher Education for Cracow University of Technology.

Data Availability Statement: Not applicable.

Conflicts of Interest: The authors declare no conflict of interest.

References

1. Chalmers, B.; Spooner, E. An axial-flux permanent-magnet generator for a gearless wind energy system. *IEEE Trans. Energy Convers.* **1999**, *14*, 251–257. [CrossRef]
2. Chen, Y.; Pillay, P.; Khan, A. PM Wind Generator Topologies. *IEEE Trans. Ind. Appl.* **2005**, *41*, 1619–1626. [CrossRef]
3. Chan, T.F.; Lai, L.L. An Axial-Flux Permanent-Magnet Synchronous Generator for a Direct-Coupled Wind-Turbine System. *IEEE Trans. Energy Convers.* **2007**, *22*, 86–94. [CrossRef]
4. Park, Y.-S.; Jang, S.-M.; Choi, J.-H.; Choi, J.-Y.; You, D.-J. Characteristic Analysis on Axial Flux Permanent Magnet Synchronous Generator Considering Wind Turbine Characteristics According to Wind Speed for Small-Scale Power Application. *IEEE Trans. Magn.* **2012**, *48*, 2937–2940. [CrossRef]
5. Caricchi, F.; Crescimbini, F. Modular Axial-Flux Permanent-Magnet Motor for Ship Propulsion Drives. *IEEE Trans. Energy Convers.* **1999**, *14*, 673–679. [CrossRef]
6. Kanuch, J.; Ferkova, Z. Design and simulation of disk stepper motor with permanent magnets. *Arch. Electr. Eng.* **2013**, *62*, 281–288. [CrossRef]
7. Gieras, J.; Wang, R.; Kamper, M. *Axial Flux Permanent Magnet Brushless Machines*; Kluwer Academic Publishers: Dordrecht, The Netherlands, 2004.
8. Kirtley, J.L. *Permanent Magnets in Electric Machines. Electric Power Principle*; John Wiley & Sons Ltd.: Hoboken, NJ, USA, 2019.
9. Zhilichev, Y.N. Three-dimensional analytic model of permanent magnet axial flux machine. *IEEE Trans. Magn.* **1998**, *34*, 3897–3901. [CrossRef]
10. Parviainen, A.; Niemelä, M.; Pyrhönen, J. Modeling of axial flux permanent-magnet machines. *IEEE Trans. Ind. Appl.* **2004**, *40*, 1333–1340. [CrossRef]
11. Azzouzi, J.; Barakat, G.; Dayko, B. Quasi-3D analytical modeling of the magnetic field of an axial flux permanent-magnet synchronous machine. *IEEE Trans. Energy Conv.* **2005**, *20*, 746–752. [CrossRef]
12. Wang, R.J.; Kamper, M.J.; Van der Westhuizen, K.; Gieras, J.F. Optimal design of a coreless stator axial flux permanent-magnet generator. *IEEE Trans. Magn.* **2005**, *41*, 55–64. [CrossRef]
13. Virtic, P.; Pisek, P.; Marcic, T.; Hadziselimovic, M.; Bojan, S. Analytical Analysis of Magnetic Field and Back Electromotive Force Calculation of an Axial-Flux Permanent Magnet Synchronous Generator with Coreless Stator. *IEEE Trans. Magn.* **2008**, *44*, 4333–4336. [CrossRef]

14. Kamper, M.J.; Wang, R.-J.; Rossouw, F.G. Analysis and performance of axial flux permanent-magnet machine with air-cored nonoverlapping concentrated stator windings. *IEEE Trans. Ind. Appl.* **2008**, *44*, 1495–1504. [CrossRef]
15. Hosseini, S.M.; Agha-Mirsalim, M.; Mirzaei, M. Design, prototyping, and analysis of a low cost axial-flux coreless permanent-magnet generator. *IEEE Trans. Magn.* **2008**, *44*, 75–80. [CrossRef]
16. Choi, J.-Y.; Lee, S.-H.; Ko, K.-J.; Jang, S.-M. Improved Analytical Model for Electromagnetic Analysis of Axial Flux Machines with Double-Sided Permanent Magnet Rotor and Coreless Stator Windings. *IEEE Trans. Magn.* **2011**, *47*, 2760–2763. [CrossRef]
17. Sung, S.-Y.; Jeong, J.-H.; Park, Y.-S.; Choi, J.-Y.; Jang, S.-M. Improved Analytical Modeling of Axial Flux Machine with a Double-Sided Permanent Magnet Rotor and Slotless Stator Based on an Analytical Method. *IEEE Trans. Magn.* **2012**, *48*, 2945–2948. [CrossRef]
18. Stamenkovic, I.; Milivojevic, N.; Schofield, N.; Krishnamurthy, M.; Emadi, A. Design, Analysis, and Optimization of Ironless Stator Permanent Magnet Machines. *IEEE Trans. Power Electron.* **2013**, *28*, 2527–2538. [CrossRef]
19. Jin, P.; Yuan, Y.; Minyi, J.; Shuhua, F.; Heyun, L.; Yang, H.; Ho, S.L. 3-D Analytical Magnetic Field Analysis of Axial Flux Permanent-Magnet Machine. *IEEE Trans. Magn.* **2014**, *50*, 11. [CrossRef]
20. Huang, Y.K.; Zhou, T.; Dong, J.N.; Lin, H.Y.; Yang, H.; Cheng, M. Magnetic equivalent circuit modeling of yokeless axial flux permanent magnet machine with segmented armature. *IEEE Trans. Magn.* **2014**, *50*, 8104204. [CrossRef]
21. Maryam, S.; Naghi, R.; Vahid, B.; Juha, P.; Majid, R. Comparison of Performance Characteristics of Axial-Flux Permanent-Magnet Synchronous Machine with Different Magnet Shapes. *IEEE Trans. Magn.* **2015**, *51*, 8115206.
22. Petrov, I.; Pyrhonen, J. Performance of Low-Cost Permanent Magnet Material in PM Synchronous Machines. *IEEE Trans. Ind. Electron.* **2013**, *60*, 2131–2138. [CrossRef]
23. Fasolo, A.; Alberti, L.; Bianchi, N. Performance Comparison Between Switching-Flux and IPM Machines with Rare-Earth and Ferrite PMs. *IEEE Trans. Ind. Appl.* **2014**, *50*, 3708–3716. [CrossRef]
24. Boldea, I.; Tutelea, L.N.; Parsa, L.; Dorrell, D. Automotive Electric Propulsion Systems with Reduced or No Permanent Magnets: An Overview. *IEEE Trans. Ind. Electron.* **2014**, *61*, 5696–5711. [CrossRef]
25. Rahman, M.M.; Kim, K.T.; Hur, J. Design and optimization of Neodymium-free SPOKE-Type motor with segmented wing-shaped PM. *IEEE Trans. Magn.* **2014**, *50*, 865–868. [CrossRef]
26. Raminosoa, T.; El-Refaie, A.; Pan, D.; Huh, K.-K.; Alexander, J.; Grace, K.; Grubic, S.; Galioto, S.; Reddy, P.B.; Shen, X. Reduced Rare-Earth Flux-Switching Machines for Traction Applications. *IEEE Trans. Ind. Appl.* **2015**, *51*, 2959–2971. [CrossRef]
27. Hua, H.; Zhu, Z.Q.; Wang, C.; Zheng, M.; Wu, Z.; Wu, D.; Ge, X. Partitioned Stator Machines with NdFeB and Ferrite Magnets. *IEEE Trans. Ind. Appl.* **2017**, *53*, 1870–1882. [CrossRef]
28. Damiano, A.; Floris, A.; Fois, G.; Marongiu, I.; Porru, M.; Serpi, A. Design of a high-speed ferrite-based brushless DC machine for electric vehicles. *IEEE Trans. Ind. Appl.* **2017**, *53*, 4279–4287. [CrossRef]
29. Johnson, M.; Gardner, M.C.; Toliyat, H.A. Design Comparison of NdFeB and Ferrite Radial Flux Surface Permanent Magnet Coaxial Magnetic Gears. *IEEE Trans. Ind. Appl.* **2018**, *54*, 1254–1263. [CrossRef]
30. Li, Y.; Yang, H.; Lin, H.; Fang, S.; Wang, W. A Novel Magnet-Axis-Shifted Hybrid Permanent Magnet Machine for Electric Vehicle Applications. *Energies* **2019**, *12*, 641. [CrossRef]
31. Tahanian, H.; Aliahmadi, M.; Faiz, J. Ferrite permanent magnets in electrical machines: Opportunities and challenges of a non-rare—Earth alternative. *IEEE Trans. Magn.* **2020**, *56*, 900120. [CrossRef]
32. Chang-Hoon, S.; Hong-Soon, C.; Jangho, S. Design and analysis of a novel spoke—Type motor to reduce the use of rare—Earth magnet materials. *IET Electr. Power Appl.* **2021**, *15*, 1479–1487.
33. Poudel, B.; Amiri, E.; Rastgoufard, P.; Mirafzal, B. Toward Less Rare-Earth Permanent Magnet in Electric Machines: A Review. *IEEE Trans. Magn.* **2021**, *57*, 900119. [CrossRef]
34. Jeong, C.; Cinti, L.; Bianchi, N. Direct Drive Applications: Possible Replacement of Rare-Earth Permanent Magnet Motors. *Energies* **2021**, *14*, 8058. [CrossRef]
35. Rao, D.; Bagianathan, M. Selection of Optimal Magnets for Traction Motors to Prevent Demagnetization. *Machines* **2021**, *9*, 124. [CrossRef]
36. Zheng, S.; Zhu, X.; Xu, L.; Xiang, Z.; Quan, L.; Yu, B. Multi-Objective Optimization Design of a Multi-Permanent-Magnet Motor Considering Magnet Characteristic Variation Effects. *IEEE Trans. Ind. Electron.* **2022**, *69*, 3428–3438. [CrossRef]
37. Yunyun, C.; Tongle, C.; Xiaoyong, Z.; Yu, D. Optimization of a New Asymmetric-Hybrid-PM Machine with High Torque Density and Low Torque Ripple Considering the Difference of Magnetic Materials. *IEEE Trans. Magn.* **2022**, *58*, 8103505. [CrossRef]
38. Bharathi, M.; Akuru, U.B.; Kumar, M.K. Comparative Design and Performance Analysis of 10 kW Rare-Earth and Non-Rare Earth Flux Reversal Wind Generators. *Energies* **2022**, *15*, 636. [CrossRef]
39. Radwan-Praglowska, N.; Wegiel, T.; Borkowski, D. Parameters identification of coreless axial flux permanent magnet generator. *Arch. Electr. Eng.* **2018**, *67*, 391–402.
40. Radwan-Pragłowska, N.; Węgiel, T.; Borkowski, D. Modeling of Axial Flux Permanent Magnet Generators. *Energies* **2020**, *13*, 5741. [CrossRef]
41. Radwan-Pragłowska, N.; Węgiel, T.; Borkowski, D. Application of the Harmonic Balance Method for Spatial Harmonic Interactions Analysis in Axial Flux PM Generators. *Energies* **2021**, *14*, 5570. [CrossRef]
42. AMF Magnetics–Commercial Offer. Available online: https://magnet.com.au/ (accessed on 10 May 2022).
43. ENES Magnesy–Commercial Offer. Available online: https://magnesy.eu/ (accessed on 10 May 2022).